25th ABCM International Congress of Mechanical Engineering
October 20-25, 2019, Uberlândia, MG, Brazil

COB-2019-0155
EVALUATION OF THE MECHANICAL BEHAVIOR OF STEELS USED IN THE SLIDE RING OF A BALL MILL OF AN IRON ORE MINING PLANT

Leonardo Barbosa Godefroid
Luiz Cláudio Cândido
Claudinei Roberto Guimarães
Sidney Cardoso Araújo
Universidade Federal de Ouro Preto, Ouro Preto, MG, Brazil
leonardo@ufop.edu.br; candido@ufop.edu.br; claudinei.guimaraes@bol.com.br; sidney@ufop.edu.br

Abstract. *This work identified the root cause of an early failure occurring in the slide ring of a ball mill used in an iron mining plant. The steel employed at this location met very strictly the ASTM-A516-G60 specification for use in pressure vessels and similar structures. The microstructure presented by this steel consisted of a totally heterogeneous distribution of ferrite grains and pearlite colonies, with variations in grain size and volume fraction. This microstructure led to the development of fatigue cracks that crossed the thickness of the slide ring. As a consequence, the iron ore pulp was contaminated with the lubricating oil, decreasing the adequate oil level and generating excessive wear on bearings and loss of pressure from the lubrication system. All these facts made impracticable the operation of the mill. Three different steels that meet the specification for application in pressure vessels were analyzed and compared with the steel of the failed mill by means of tension, Rockwell hardness, Charpy impact, fracture toughness (J-R curves) and fatigue tests (σ_a-N_f curves and da/dN x ΔK curves). It was concluded that the material selection for the mill component must take into account a suitable chemical composition and microstructure for that application, as well as its sensitivity to high temperatures from a welding process, in order to guarantee a microstructure and a minimum of mechanical resistance compatible with its use.*

Keywords: *Failure analysis; Fatigue cracking; Ball mill; Structural steels.*

1. INTRODUCTION

Grinding ball mills are rotary equipments commonly present in iron ore mining plants, which use steel balls to reduce the ore particle size and prepare the ore pulp for subsequent concentration process. The ball mill is basically a large cylinder consisting of a shell, two slide rings which are supported on sliding bearing shoes and two heads. All structural steel members of the cylinder are joined by full penetration welds. Fig. 1 shows schematically a ball mill and presents photos of its main parts. The design of ball mills is based on methodologies adopted by international codes, for example ASME (2010), taking into account fatigue degradation due to the principle of the mills operation (Dong and Hong, 2004; Hobbacher, 2009) and an accurate analysis by finite elements (Meimaris and Lai, 2012). The mills are designed to be durable for an unlimited service life. Nevertheless, depending on numerous factors (Neves et al., 2016), such as inappropriate design (dimensioning, material selection), manufacturing (steel production, welding), poor maintenance and inadequate operating procedures (overloads, high temperature), flaws are developed in the structural components of this equipment.

This work evaluated the root cause of an early failure occurring at one of the slide rings of a ball mill used in an iron ore mining plant. This slide ring is located at the extremity of the shell which receives the grinding ore pulp, and where is operating the mechanical transmission system of the mill, near the region where the head is welded at 90^0 with the longitudinal axis of the shell. In this case, three high-length cracks separated approximately by 120^0 emerged and crossed the thickness of the slide ring after a relatively short working time. As a consequence, the iron ore pulp was contaminated with the lubricating oil, decreasing the adequate oil level and generating excessive wear on bearings and loss of pressure from the lubrication system. All these facts made impracticable the operation of the mill. The steel used in the construction of the structural component and other three steels that also meet the required specification for the mill design were characterized in terms of their chemical composition, microstructure and mechanical properties, including fatigue strength (initiation and crack growth).

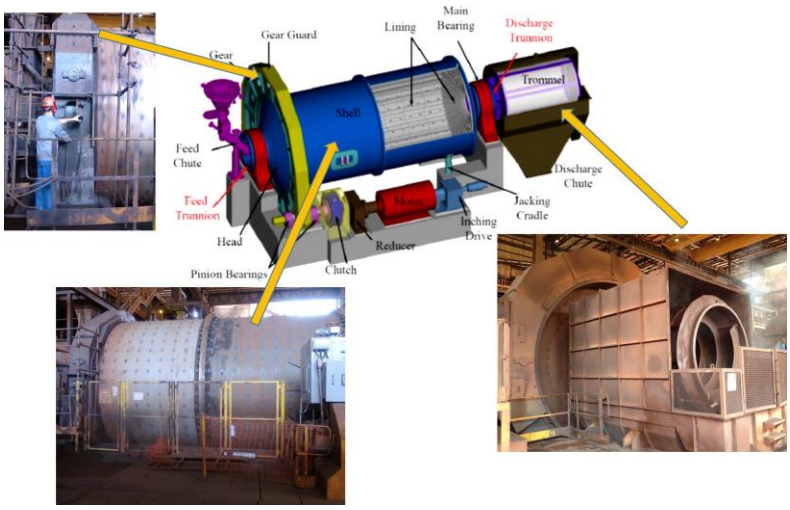

Figure 1. Scheme of a ball mill, Neves et al. (2016), and illustrative photos of its main parts.

2. MATERIALS AND METHODOLOGY

The materials studied in this work are controlled by an ASTM (2013) specification for steel plates used in pressure vessels. These are C-Mn-Si steels with ferrite/pearlite microstructure. The steel of the failed mill must meet the ASTM A516 G60 specification. Three other similar steels for the same application, purchased directly from the manufacturer and meeting the ASTM A516 G60, ASTM G70 and ASTM A285 specifications, respectively, were also considered for comparison purposes.

The failure analysis of the steel used in the mill followed the standard procedures to find the root cause of the problem: macroscopic and fractographic analysis of the cracked region, chemical composition, microstructural analysis and mechanical tests (tension, hardness, impact, fracture toughness, fatigue (initiation and crack growth)). The other steels followed a similar methodology.

The chemical composition of all steels was determined by optical emission spectrometry (OES). Samples were obtained and analyzed from the head of the fractured tension test specimens.

The microstructural characterization (ferrite grain size - d and pearlite volume fraction - V) from the steel of the failed mill used samples removed near the cracked region. All the samples were cut, ground, polished and etched with 2% Nital solution. The samples were examined using a LEICA light optical microscope (LOM) and a TESCAN VEGA3 scanning electron microscope (SEM).

All the mechanical tests were performed at room temperature in atmospheric air. Specimens from the steel of the failed mill were obtained near the cracked region. Tensile tests (ASTM, 2016), fracture toughness (J-R curve) tests (ASTM, 2018) and fatigue tests (σ_a x N_f - ASTM, 2015a; da/dN x ΔK – ASTM, 2015b) were conducted on a 100kN MTS servo-hydraulic materials testing system interfaced to a computer for machine control and data acquisition. Rockwell hardness tests were conducted on a WOLPERT machine (ASTM, 2018). Charpy impact tests were conducted on a AMSLER machine (ASTM, 2018), using sub-size specimens. The analysis of fracture surfaces was performed by a scanning electron microscope (SEM) in the steel of the failed mill and in all specimens after mechanical tests to identify and confirm the fracture mechanism of the materials.

3. RESULTS AND DISCUSSION

Fig. 2 presents a schematic representation of three cracks appearing on the slide ring in the transversal section of the ball mill. Figs. 3a and 3b are pictures showing details of the failure region. Fig. 4 presents a detail of the slide ring, showing part of one of the cracks that developed in the mill. Below this ring and close to the region of the crack is the welded head of the mill. The cracked region was subsequently separated for examination of the fractured surfaces. Some examples can be seen in Figs. 5a and 5b. From the details observed in this macroscopic analysis (flat surface and beach marks), and taking into account the characteristic operation of the equipment, it is clear that the failure was caused by fatigue.

Table 1 shows the chemical composition of all steels studied. The steel of the failed mill has met the corresponding ASTM specification for the original design, very close to the specified limits. It should be emphasized that a composition with higher carbon and alloying elements content could result in a more refined microstructure and more suitable mechanical properties for the proposed application. The other steels used for comparison are in accordance with the ASTM specifications.

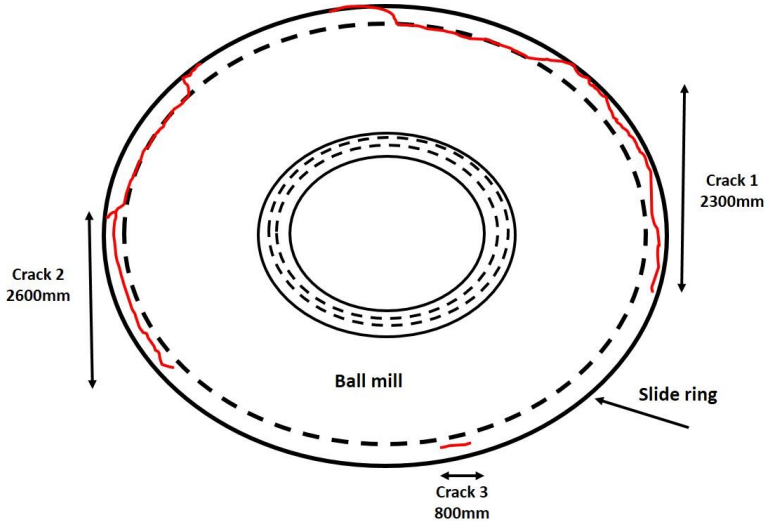

Figure 2. Schematic representation of three cracks appearing on the slide ring, transversal section of the ball mill.

(a) (b)

Figure 3. Pictures showing details of the failure region.

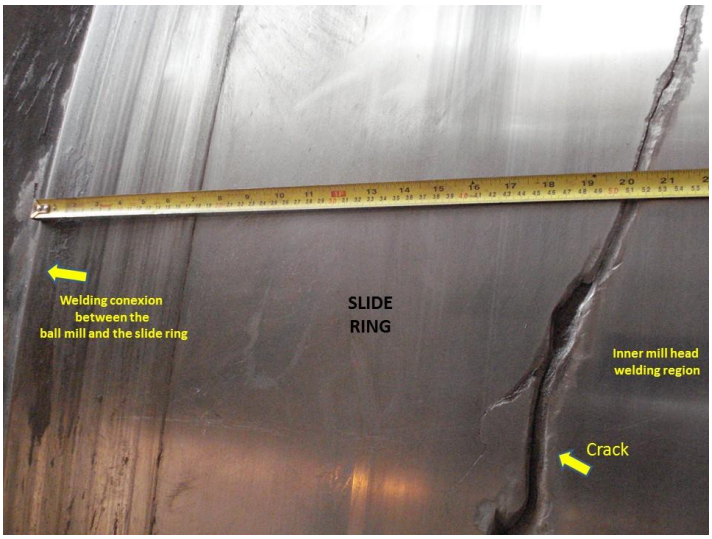

Figure 4. Development of one of the cracks near a welding region.

.

(a) (b)

Figure 5. Fracture surfaces after forced opening of the cracks.

Table 1: Chemical composition of all steels (wt%).

Grade	C	Mn	Si	P	S	Cr	Ni	Mo	Al	Nb+Ti+V
Failed steel	0.15	1.05	0.24	0.017	0.003	0.03	0.01	-	0.05	0.02
ASTM G60	0.18	1.15	0.21	0.026	0.005	0.01	0.01	0.02	0.03	0.01
ASTM G70	0.20	1.13	0.20	0.027	0.006	0.01	0.01	0.02	0.03	0.01
ASTM A285	0.14	0.68	0.22	0.023	0.008	0.01	0.01	0.02	-	0.01

Figs. 6a and 7a show the microstructure of the failed mill steel. As expected, it consists of a ferrite and pearlite mixture. The distribution and size of the phase/constituent is significantly heterogeneous, which obviously will influence the mechanical properties of the material. The microstructure of the steels used for comparison is shown in Figs. 6b, 6c, 6d and 7b, 7c, 7d. All these three steels have a typical hot rolling microstructure, with smaller phase/constituent size than the mill steel. Table 2 presents the ferrite grain size and volume fraction of all steels. The heterogeneous microstructure of the steel used in the mill is most likely the result of an erroneously conducted manufacturing process. The welding operation for fixing the head to the shell helped to deteriorate this microstructure, with high heat input in this region.

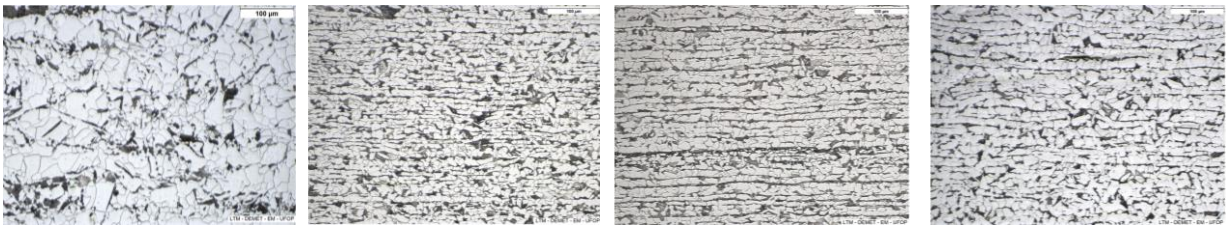

(a) Failed mill steel (b) ASTM 516 G60 (c) ASTM 516 G70 (d) ASTM A285

Figure 6. Microscopical analysis of the studied steels. LOM. 2% Nital. Original magnification = 200X.

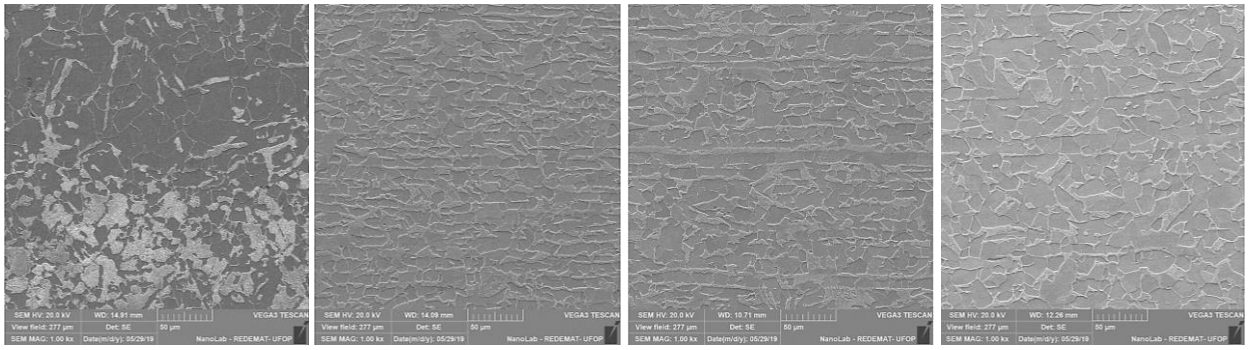

(a) Failed mill steel (b) ASTM 516 G60 (c) ASTM 516 G70 (d) ASTM A285

Figure 7. Microscopical analysis of the studied steels. SEM. 2% Nital. Original magnification = 1000X.

Table 2: Quantitative metallography results, steels used in mills.

Grade	Failed mill steel	ASTM 516 G60	ASTM 516 G70	ASTM A285
d (μm)	12 ± 3	8 ± 1	8 ± 2	9 ± 1
V (%)	30 ± 5	40 ± 3	48 ± 4	39 ± 6

Table 3 shows results obtained in tensile, hardness and impact tests. All steels showed a behavior in accordance with the corresponding ASTM specification. It is possible to see that all steels have characteristics of ductility, a fact verified by fractographic analysis. It can be observed that the steel of the failed mill has a significantly lower tensile strength and hardness than the other steels, including the identical steel specified for the mill (ASTM A516 G60). On the other hand, the energy absorbed in the impact test is much higher than the values found for the other steels. These facts are a consequence of the heterogeneous and coarser microstructure, and certainly imply in its behavior in service.

Table 3: Mechanical properties: tensile tests, hardness tests, Charpy impact tests; room temperature.

Grade	**YS (MPa)**	**UTS (MPa)**	**ELO (%)**	**AR (%)**	**HRc**	**AE (J)**	**LE (%)**
Failed mill steel	252 ± 1	449 ± 9	45 ± 6	72 ± 3	23 ± 0,6	76 ± 9,3	26 ± 1,2
ASTM A516 G60	406 ± 7	574 ± 2	42 ± 2	67 ± 2	28 ± 0,9	43 ± 0,4	21 ± 0,7
ASTM A516 G70	399 ± 4	563 ± 6	43 ± 4	61 ± 4	27 ± 0,5	45 ± 1,5	23 ± 0,2
ASTM A285	347 ± 10	465 ± 4	45 ± 5	63 ± 1	24 ± 0,7	34 ± 1,0	18 ± 1,1

YS: Yield Strength; UTS: Ultimate Tensile Strength; ELO: Total strain; AR: Area Reduction; HRc: Rockwell C Hardness; AE: Charpy Absorbed Energy; LE: Charpy Lateral Expansion.

Figure 8 shows crack resistance curves for all steels, in the form of variation of the J integral with the crack advance. This is an average of three fracture toughness tests for each steel. The best performance of failed mill steel can be observed. This higher value for fracture toughness was already expected, from the knowledge of its ductile performance in tensile, hardness and impact tests. A more ductile material will develop a larger plastic zone at the crack tip, with corresponding larger field of residual compressive stresses, shielding its propagation (Anderson, 2017). Figure 9 shows the fracture surface of test specimens corresponding to the four steels, immediately ahead of fatigue pre-crack. The ductile behavior of all steels can be confirmed, more predominant in the failed mill steel, with the characteristic presence of dimples.

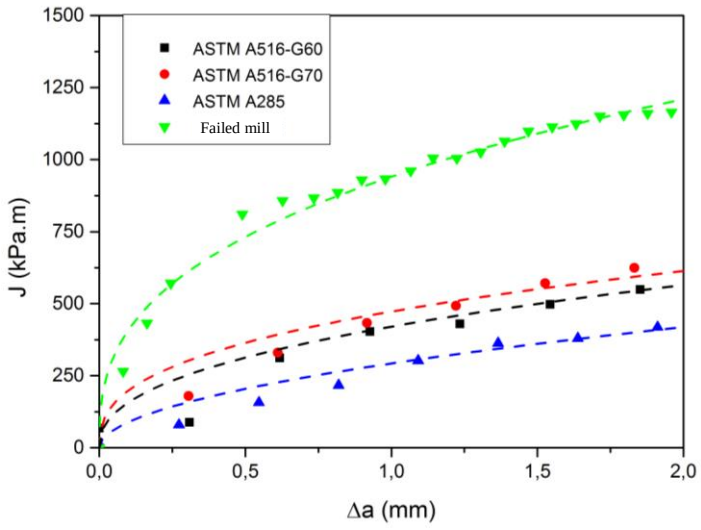

Figure 8. Fracture toughness for all steels. The dashed curves are trend adjustments.

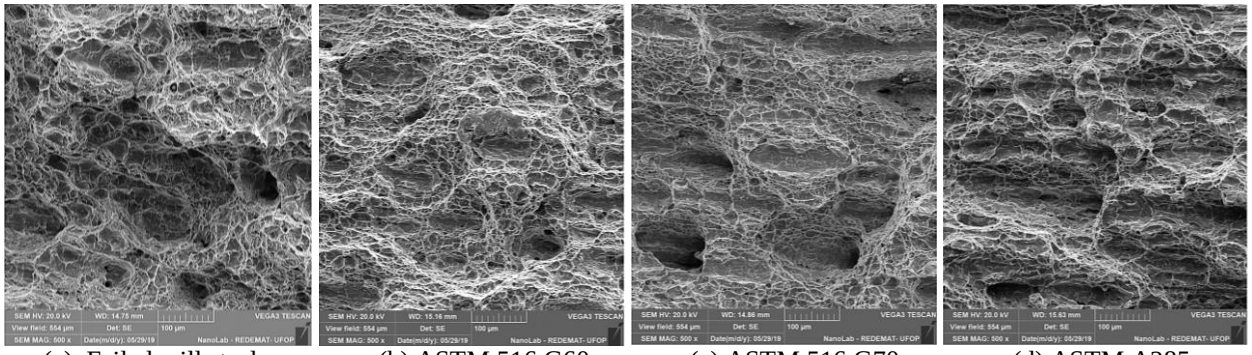

(a) Failed mill steel (b) ASTM 516 G60 (c) ASTM 516 G70 (d) ASTM A285

Figure 9. Fracture surface of the fracture toughness specimens. SEM. Original magnification = 500X.

Figure 10 shows the results obtained in constant amplitude fatigue-life tests with all studied steels. It can be observed that the steel used in the mill presented a lower performance in relation to the ASTM A516 G60 and G70 steels with respect to the crack initiation resistance. This behavior is related to the difference of microstructures between the steels (Schijve, 2009; Suresh, 1998). A more ductile steel with lower tensile strength is more sensitive to nucleate fatigue cracks than more resistant steels due to the greater ease of developing intrusions/extrusions on its surface. This fact explains the early appearance of cracks in the slide ring of the mill. The failed mill steel with its coarse and heterogeneous microstructure allows the nucleation of fatigue cracks. As the mill works under cyclic loading, its failure becomes unavoidable after a certain operational period. With respect to the cracking mechanism, all steels showed the basic sequence of nucleation in one of the corners of the specimen (roughness surface), growth (striations) and final tensile rupture (ductile), as shown in Figure 11 for the failed steel.

Figure 12 characterizes the fatigue crack growth resistance of all studied steels. The steel of the mill presented a higher fatigue crack growth resistance than the other steels studied, again due to its microstructure (Schijve, 2009; Suresh, 1998). In this case, the behavior of the material resembles the performance in fracture toughness tests. In the region of the fatigue threshold, roughness/oxidation and later plasticity crack closure mechanisms shield the crack growth, increasing the fatigue strength of the material. With respect to the cracking mechanism, all steels showed the basic sequence of a roughness surface at the threshold region, striations at the linear curve and final ductile rupture, as shown in Figure 13 for the failed steel.

If material selection was only performed with parameters linked to fatigue crack growth, the failed steel could be considered relatively safe. However, considering the operational complexity of the mill and the consequent need to minimize the appearance of cracks, one can conclude that it would be safer to work with a more resistant steel, both in terms of tensile and fatigue crack initiation.

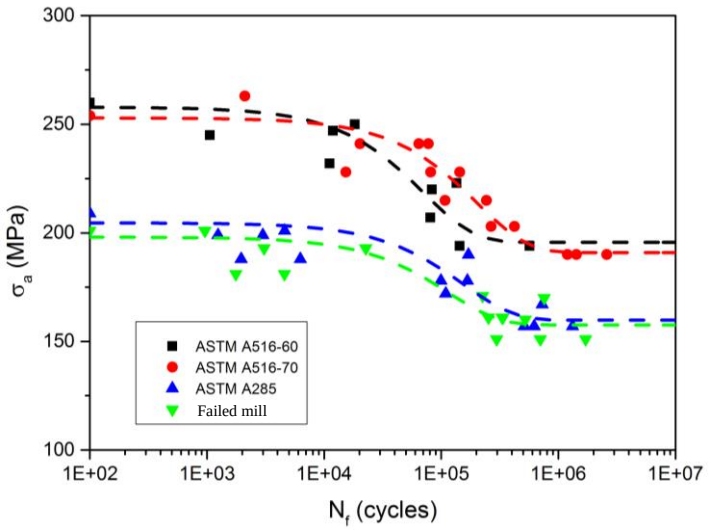

Figure 10. Constant amplitude fatigue-life curves of steels used in mills. The dashed curves are trend adjustments.

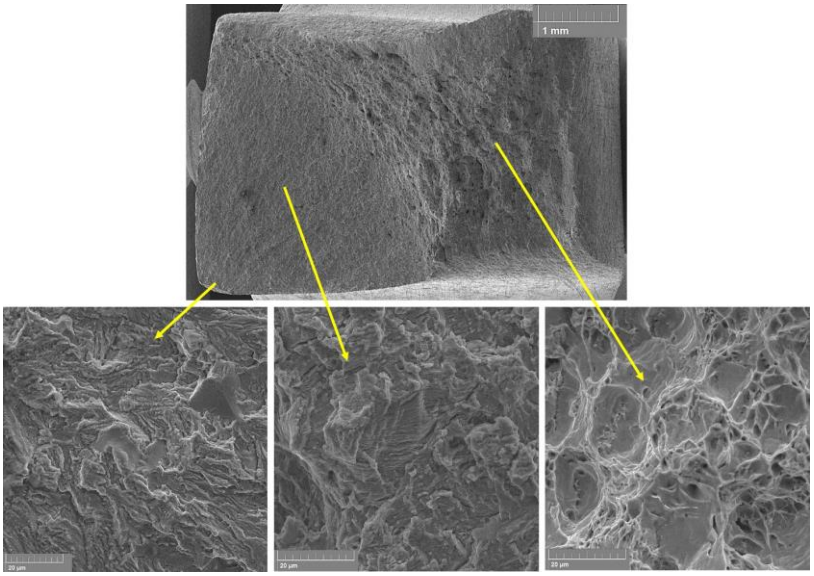

Figure 11. Fracture surface of a constant amplitude fatigue-life specimen, corresponding to the failed mill steel. SEM.

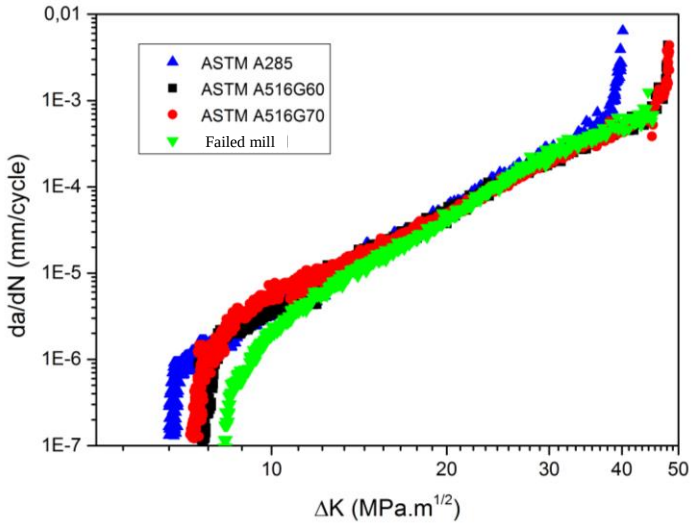

Figure 12. Fatigue crack growth curves of steels used in mills.

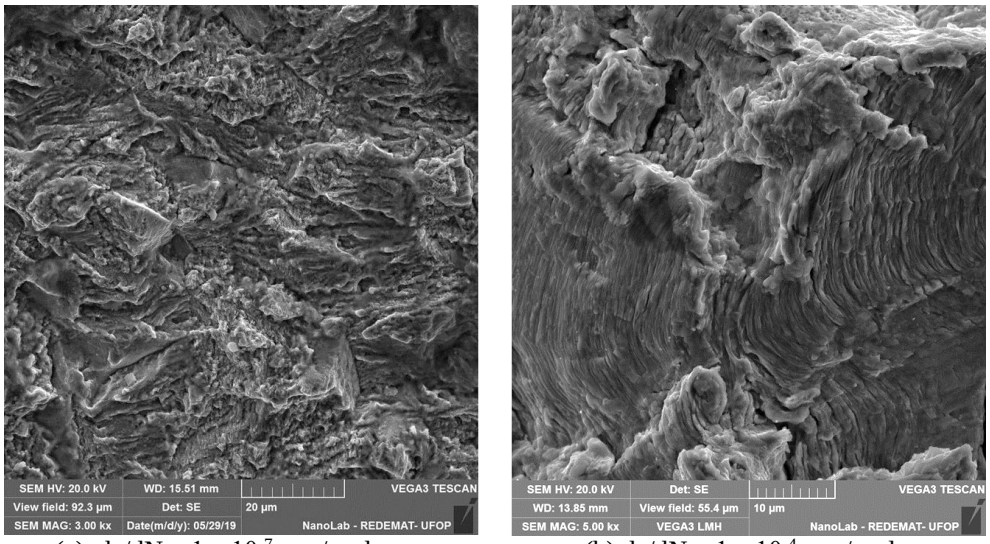

(a) da/dN ≈ 1 x 10^{-7} mm/cycle. (b) da/dN ≈ 1 x 10^{-4} mm/cycle.

Figure 13. Fracture surface of a fatigue crack growth specimen, corresponding to the failed mill steel. SEM.

4. CONCLUSIONS

The material selection for the mill component must take into account a suitable chemical composition and microstructure for that application, as well as its sensitivity to high temperatures from a welding process, in order to guarantee a microstructure and a minimum of mechanical resistance compatible with its use. In this work, it was verified that the heterogeneous microstructure of the steel used in the mill is most likely the result of an erroneously conducted manufacturing process. The welding operation for fixing the head to the shell helped to deteriorate this microstructure, with high heat input in this region. The manufacturing process and the welding procedure altered significantly the appropriate microstructure of the specified steel, reducing its tensile strength and, consequently, its resistance to fatigue crack nucleation.

5. REFERENCES

Anderson, T.L., 2017. “Fracture Mechanics – Fundamentals and Applications”, CRC Press.
ASME, 2010. “Boiler and Pressure Vessel Code. Section XI, Rules for In-service Inspection of Nuclear Power Plant Components”. (Appendix A).
ASTM, 2010. “Standard Specification for Pressure Vessel Plates, Carbon Steel, for Moderate- and Lower-Temperature Service”.
ASTM, 2015a. “Standard Practice for Conducting Force Controlled Constant Amplitude Axial Fatigue Tests of Metallic Materials”.
ASTM, 2015b. “Standard Test Method for Measurement of Fatigue Crack Growth Rates”.
ASTM, 2016. “Standard Test Methods for Tension Testing of Metallic Materials”.
ASTM 2018. “Standard Test Method for Measurement of Fracture Toughness”.
ASTM, 2018. “Standard Test Methods for Rockwell Hardness of Metallic Materials”.
ASTM, 2018. “Standard Test Methods for Notched Bar Impact Testing of Metallic Materials”.
Dong, P., Hong, J.K., 2004. “The master S-N curve approach to fatigue evaluation of offshore and marine structures”. *Proceedings of OMAE04: 23rd International Conference on Offshore Mechanics and Arctic Engineering.*
Hobbacher, A.F., 2009. “The new IIW recommendations for fatigue assessment of welded jointsand components – A comprehensive code recently updated”. *International Journal of Fatigue*, Vol. 31, pp. 50–58.
Meimaris, C., Lai, W.K.K., 2012. “Fatigue design of mills”. *Minerals Engineering*, Vol. 30, pp. 52–61.
Neves, M.D.M., Andrade, A.H.P., Silva, D.N., 2016. “Analysis of the criticality of flaws found in trunnion of grinding ball mills used in mining plants”. *Engineering Failure Analysis,* Vol. 61, pp. 28–36.
Schijve, J., 2009. “Fatigue of Structures and Materials”, Springer.
Suresh, S., 1998. “Fatigue of Materials”, Cambridge University Press

6. RESPONSIBILITY NOTICE

The authors are the only responsible for the printed material included in this paper.